



Deposited via The University of York.

White Rose Research Online URL for this paper:

<https://eprints.whiterose.ac.uk/id/eprint/134151/>

Version: Accepted Version

---

**Article:**

Clark, Nick, Nguyen, Lan, Hamer, Matthew J. et al. (2018) Scalable Patterning of Encapsulated Black Phosphorus. Nano Letters. ISSN: 1530-6984

<https://doi.org/10.1021/acs.nanolett.8b00946>

---

**Reuse**

Items deposited in White Rose Research Online are protected by copyright, with all rights reserved unless indicated otherwise. They may be downloaded and/or printed for private study, or other acts as permitted by national copyright laws. The publisher or other rights holders may allow further reproduction and re-use of the full text version. This is indicated by the licence information on the White Rose Research Online record for the item.

**Takedown**

If you consider content in White Rose Research Online to be in breach of UK law, please notify us by emailing [eprints@whiterose.ac.uk](mailto:eprints@whiterose.ac.uk) including the URL of the record and the reason for the withdrawal request.

## Scalable Patterning of Encapsulated Black Phosphorus

Nick Clark, Lan Nguyen, Matthew J. Hamer, Fredrik Schedin, Edward A Lewis, Eric Prestat, Alistair Garner, Yang Cao, Mengjian Zhu, Reza J. Kashtiban, Jeremy Sloan, Demie M. Kepaptsoglou, Roman Vladislavovich Gorbachev, and Sarah J. Haigh

*Nano Lett.*, **Just Accepted Manuscript** • DOI: 10.1021/acs.nanolett.8b00946 • Publication Date (Web): 01 Aug 2018

Downloaded from <http://pubs.acs.org> on August 3, 2018

### Just Accepted

“Just Accepted” manuscripts have been peer-reviewed and accepted for publication. They are posted online prior to technical editing, formatting for publication and author proofing. The American Chemical Society provides “Just Accepted” as a service to the research community to expedite the dissemination of scientific material as soon as possible after acceptance. “Just Accepted” manuscripts appear in full in PDF format accompanied by an HTML abstract. “Just Accepted” manuscripts have been fully peer reviewed, but should not be considered the official version of record. They are citable by the Digital Object Identifier (DOI®). “Just Accepted” is an optional service offered to authors. Therefore, the “Just Accepted” Web site may not include all articles that will be published in the journal. After a manuscript is technically edited and formatted, it will be removed from the “Just Accepted” Web site and published as an ASAP article. Note that technical editing may introduce minor changes to the manuscript text and/or graphics which could affect content, and all legal disclaimers and ethical guidelines that apply to the journal pertain. ACS cannot be held responsible for errors or consequences arising from the use of information contained in these “Just Accepted” manuscripts.



# Scalable Patterning of Encapsulated Black Phosphorus

*Nick Clark<sup>1†</sup>, Lan Nguyen<sup>1†</sup>, Matthew J. Hamer<sup>2</sup>, Fredrik Schedin<sup>3</sup>, Edward A. Lewis<sup>1</sup>, Eric Prestat<sup>1</sup>, Alistair Garner<sup>1</sup>, Yang Cao<sup>2</sup>, Mengjian Zhu<sup>2</sup>, Reza Kashtiban<sup>4</sup>, Jeremy Sloan<sup>4</sup>, Demie Kepaptsoglou<sup>5</sup>, Roman V. Gorbachev<sup>2+</sup>, Sarah J. Haigh<sup>1\*</sup>*

1. School of Materials, University of Manchester, Oxford Road, M13 9PL, United Kingdom

2. School of Physics and Astronomy, University of Manchester, Oxford Road, M13 9PL, United Kingdom

3. National Graphene Institute, University of Manchester, Oxford Road, M13 9PL, United Kingdom

4. Department of Physics, University of Warwick, Coventry, CV4 7AL, United Kingdom

5. SuperSTEM Laboratory, STFC Daresbury Campus, Daresbury, WA4 4AD, United Kingdom

<sup>†</sup>Both authors contributed equally

Corresponding Authors: [\\*sarah.haigh@manchester.ac.uk](mailto:*sarah.haigh@manchester.ac.uk); [+roman@manchester.ac.uk](mailto:+roman@manchester.ac.uk)

## KEYWORDS

Phosphorene, Graphene encapsulation, van der Waals heterostructures, Direct Write Oxidation, Transmission Electron Microscopy, Electron Beam sculpting, Local Oxidation Lithography

1  
2  
3 ABSTRACT  
4  
5  
6

7 Atomically thin black phosphorus (BP) has attracted considerable interest due to its unique properties, such as  
8 an infrared band gap that depends on the number of layers and excellent electronic transport characteristics.

9  
10 This material is known to be sensitive to light and oxygen and degrades in air unless protected with an  
11 encapsulation barrier, limiting its exploitation in electrical devices. We present a new scalable technique for  
12 nano-patterning few layer thick BP crystals by direct electron beam exposure of encapsulated crystals  
13 achieving a spatial resolution down to 6 nm. By encapsulating the BP with single layer graphene or hexagonal  
14 boron nitride (hBN), we show that a focused electron probe can be used to produce controllable local oxidation  
15 of BP through nanometre size defects created in the encapsulation layer by the electron impact. We have tested  
16 the approach in the scanning transmission electron microscope (STEM) and using industry standard electron  
17 beam lithography (EBL). Etched regions of the BP are stabilized by a thin passivation layer and demonstrate  
18 typical insulating behavior as measured at 300 K and 4.3 K. This new scalable approach to nano-patterning of  
19 thin air sensitive crystals has the potential to facilitate their wider use for a variety of sensing and electronics  
20 applications.  
21  
22  
23  
24  
25  
26  
27  
28  
29  
30  
31  
32  
33  
34  
35  
36  
37  
38  
39  
40  
41  
42  
43  
44  
45  
46  
47  
48  
49  
50  
51  
52  
53  
54  
55  
56  
57  
58  
59  
60

1  
2  
3 INTRODUCTION  
4

5 The successful isolation of few-layer black phosphorus (BP) has generated remarkable excitement in a very  
6 short time.<sup>1-3</sup> Such isolation is possible due to its highly anisotropic crystal structure where corrugated layers  
7 of phosphorous atoms are bonded by weak van-der-Waals interactions and can be easily separated. Using a  
8 similar strategy to that of graphene, atomically thin layers of BP can be extracted from the bulk by mechanical  
9 exfoliation<sup>4-6</sup> and by liquid phase exfoliation<sup>7-9</sup>. As it is made progressively thinner, the direct band gap in BP  
10 varies from ~0.3 eV in bulk to ~1.5 eV for a monolayer.<sup>4, 10-14</sup> Crystals only a few nanometers thick  
11 demonstrate high carrier mobility (reported hole mobility of 5200 cm<sup>2</sup>V<sup>-1</sup>s at room temperature and 45000  
12 cm<sup>2</sup>V<sup>-1</sup>s below 20K)<sup>15</sup> ) and high on-off ratios in field-effect devices (up to 10<sup>5</sup>)<sup>5, 16-17</sup> offering potential for  
13 applications in high-speed optoelectronic devices.<sup>2, 5, 17-20</sup> Black phosphorous is a complementary addition to  
14 the 2D materials library, providing a variable band gap between those of graphene (no band gap) and  
15 semiconducting 2D-dichalcogenides (which lie between 1.3-2 eV). Nonetheless, the exploitation of BPs  
16 electronic properties is hampered by the materials strong susceptibility to oxidation<sup>21</sup> in the presence of air.  
17 This degradation is amplified by humidity, exposure to light and elevated temperatures<sup>6, 22-25</sup> leading to a  
18 drastic deterioration of BPs electronic and optical properties.<sup>24-25</sup> The observed degradation rate increases for  
19 thinner BP flakes,<sup>26</sup> with monolayers visibly degrading over the course of a few minutes and even relatively  
20 thick (10 nm) crystals degrading to form droplet-like oxidation bubbles within 24 hours in air.<sup>4, 6, 24-25, 27</sup> The  
21 etching process in thicker flakes (>50 nm) is observed to self-terminate after a few days due to the  
22 accumulation of oxidized phosphorus (P<sub>x</sub>O<sub>y</sub>) forming a protective layer on the surface of the flake<sup>28</sup>.

23  
24  
25  
26  
27  
28  
29  
30  
31  
32  
33  
34  
35  
36  
37  
38  
39  
40  
41  
42  
43 Reduced degradation of BP has been achieved using a number of different methods including deliberate  
44 generation of a protective surface oxide layer through plasma etching<sup>29</sup>, coating with alumina,<sup>25, 30-31</sup>  
45 polymers<sup>6, 30</sup> and ionic liquids<sup>32-33</sup> but perhaps most promising method for electronic device applications is the  
46 encapsulation with 2D materials such as graphene<sup>34</sup> or hBN.<sup>16, 34-36</sup> These materials provide an ultrathin,  
47 chemically robust and impermeable barrier to anything larger than a single proton.<sup>37</sup> Precise patterning of BP  
48 nanoribbons has been proposed as a route to tuning the band gap and electronic properties by controlling  
49 orientation, width and edge terminations.<sup>38-42</sup> Drndić et al<sup>43-44</sup> have reported nanoscale sculpting of many-layer  
50  
51  
52  
53  
54  
55  
56  
57  
58  
59  
60

1  
2  
3 (17 nm thick) BP nanoribbons using direct write electron beam ablation in the STEM. Unfortunately the  
4  
5 theoretically predicted transport properties could not be verified experimentally and the ribbon would have  
6  
7 been susceptible to atmospheric degradation on removal from the high vacuum of the STEM.<sup>43</sup> Additionally, it  
8  
9 is important to consider the potential effect of electron beam irradiation on the BP structure, both in the context  
10  
11 of STEM patterning and for the more scalable approach of EBL processing.  
12  
13  
14

15 Here, we develop a scalable protocol to controllably sculpt BP devices using EBL and graphene or hBN  
16  
17 encapsulation. We demonstrate that introducing atomic scale defects in the encapsulation layer with a focused  
18  
19 electron beam allows air species to come into contact with selected areas of the embedded BP crystal and  
20  
21 generate a few-nanometer oxide region around the perforation point. We induce such local oxidation  
22  
23 controllably within both STEM and EBL instruments and use electron diffraction, energy dispersive X-ray  
24  
25 spectroscopy (EDXS) and electron energy loss spectroscopy (EELS) to study the atomic and chemical  
26  
27 structure of the etched locations. After prolonged exposure to ambient conditions, the patterns have a smallest  
28  
29 feature size of 6 nm (STEM) and 10 nm (EBL). Such resolution is extremely difficult to achieve using other  
30  
31 traditional masking and etching techniques used in semiconductor fabrication due to the necessity of using  
32  
33 polymer resists. We further show that oxidized lines as narrow as 10 nm demonstrate clear insulating behavior  
34  
35 with a breakdown voltage well above that of vacuum even at room temperature.  
36  
37  
38  
39  
40  
41  
42  
43  
44  
45  
46  
47  
48  
49  
50  
51  
52  
53  
54  
55  
56  
57  
58  
59  
60

1  
2  
3 RESULTS/DISCUSSION  
4

5 The experimental BP samples were mechanically exfoliated from bulk crystals in a clean argon glovebox to  
6 avoid oxidation.<sup>39</sup> Thin flakes of few layer BP were identified using their optical contrast and then sandwiched  
7 between two graphene (G) or hBN crystals. For STEM experiments, monolayer graphene or hBN sheets were  
8 used to encapsulate thin (2-5 layer) BP flakes, which were then transferred to a TEM support film. The full  
9 encapsulation and transfer procedure was performed immediately after the BP exfoliation in the same argon  
10 chamber via the van der Waals pick-up technique<sup>45-46</sup> using our specially developed motorized  
11 micromanipulation stage.<sup>47-49</sup>  
12  
13  
14  
15  
16  
17  
18  
19  
20  
21  
22  
23  
24  
25  
26  
27  
28  
29  
30  
31  
32  
33  
34  
35  
36  
37  
38  
39  
40  
41  
42  
43  
44  
45  
46  
47  
48  
49  
50  
51  
52  
53  
54  
55  
56  
57  
58  
59  
60

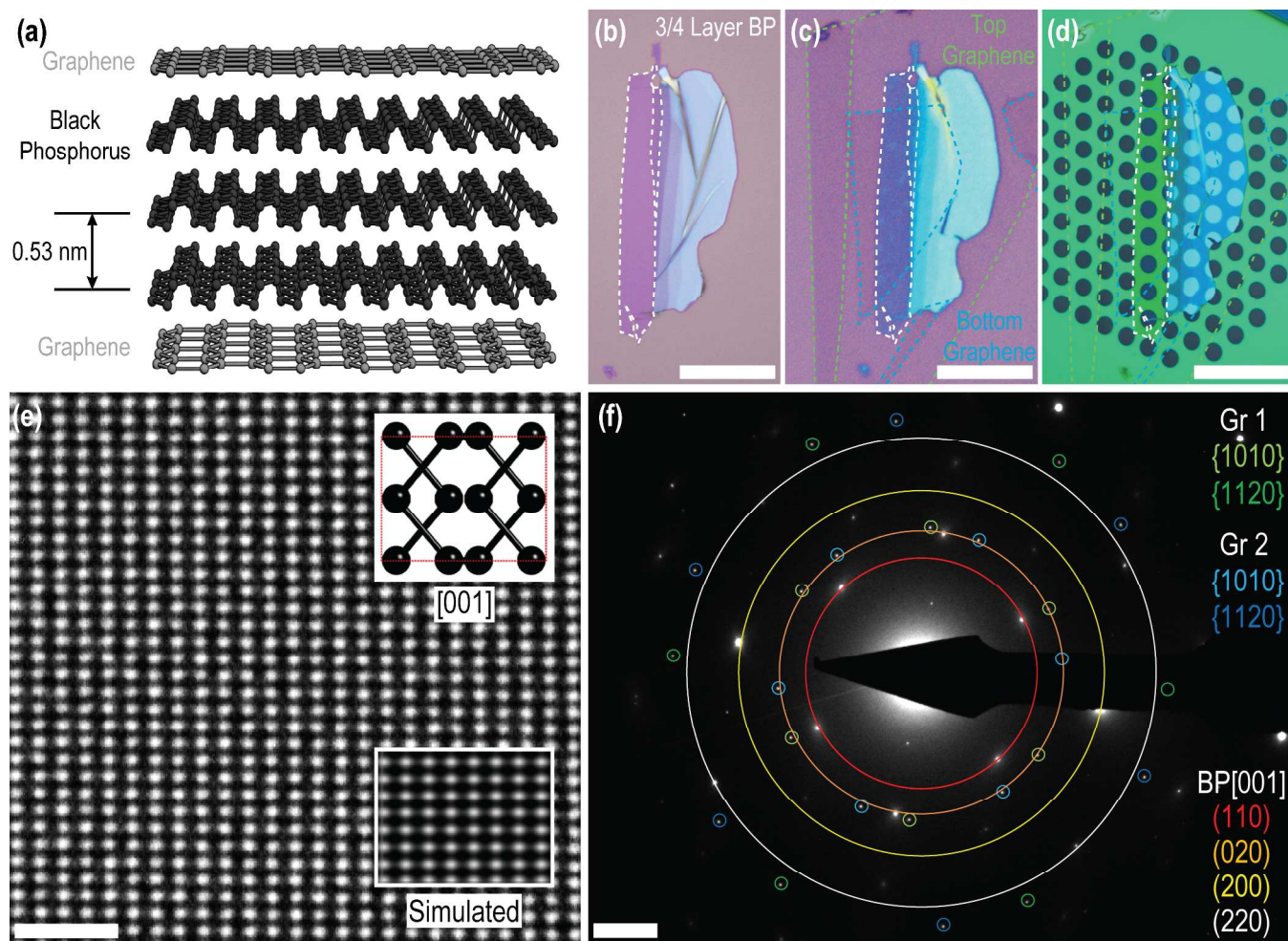


Figure 1: (a) Schematic of the graphene-encapsulated BP sample. (b) Optical micrograph of a 3-4 layer BP flake after exfoliation on an oxidized silicon substrate. (c) The same BP flake after top and bottom graphene encapsulation. The dashed lines highlight edges of mechanically exfoliated crystals. All exfoliation and transfer is performed in an argon environment glove box to prevent oxidation of BP during the sample fabrication. (d) The same sample after transfer to a silicon nitride TEM support film. Scale bars for (b)-(d) are 20  $\mu\text{m}$ . (e) Atomic-resolution Wiener-filtered aberration-corrected TEM image of a 5-layer thick area of pristine BP flake. The insets show an image simulation and ball-and-stick model of the [001] orientation. Scale bar is 1 nm. (f) Diffraction pattern from the area imaged in (e), showing two sets of spots corresponding to the upper and lower graphene sheets (misoriented by  $\sim 20^\circ$ ), and the expected BP diffraction spots. The inner BP spots are forbidden reflections which are only visible in few-layered BP flakes. (See supporting information Figure S3 for diffraction pattern without overlays). Scale bar is 2  $\text{nm}^{-1}$ .

1  
2  
3 Figure 1b shows an optical micrograph of an exfoliated BP flake prior to encapsulation. Thin BP flakes  
4 deposited on thin thermal silicon oxide layers exhibit an enhanced optical contrast with a constant contrast  
5 difference as the layer number is increased, making it simple to identify layer numbers in exfoliated flakes<sup>50</sup>, as  
6 with other 2D materials<sup>51-52</sup>. Figures 1c and 1d show the same BP flake (from figure 1b) after encapsulation  
7 within a G/BP/G stack on an oxidized silicon wafer and after transfer onto a silicon nitride support grid  
8 respectively. Atomic-resolution TEM images obtained at many locations across such encapsulated crystals  
9 show the long-range pristine atomic structure of BP with no visible lattice defects in few layer crystals after 5  
10 months of storage in air. Low magnification high angle annular dark field (HAADF) STEM images of a  
11 previously unimaged area after encapsulation for more than 6 months are included in Figure S6 in the  
12 supporting material. Figure 1e shows a typical TEM image where the atomic lattice is clearly visible even  
13 without filtering out the spatial frequencies of the encapsulating graphene layers. The high crystal quality of  
14 our samples is further confirmed with electron diffraction, as shown in Figure 1f. The spots marked with blue  
15 and green are the  $\{10\bar{1}0\}$  and  $\{11\bar{2}0\}$  reflections for two single layer graphene sheets with the upper and lower  
16 graphene lattices twisted relative to each other by  $\sim 20^\circ$ . Figure 1e also contains the expected spot pattern for  
17 BP viewed along  $[001]$  where the lattice parameters are  $a = 3.31 \text{ \AA}$ ,  $b = 4.38 \text{ \AA}$  and  $c = 10.5 \text{ \AA}$ , as defined by  
18 Hultgren.<sup>53</sup> We note that other works have defined the unit cell with the b-axis being longest.<sup>4, 22, 54-56</sup> The  
19 number of layers in our BP samples can be confirmed using the ratio of the  $(110)/(200)$  spot intensities in the  
20 diffraction pattern.<sup>4</sup> For the sample presented in Figure 1 the ratio was found to be  $\sim 0.1$ , confirming that this  
21 area of BP crystal is 5 layers thick ( $\sim 2.6 \text{ nm}$ , see Figure S3 in supporting material).

22  
23  
24  
25  
26  
27  
28  
29  
30  
31  
32  
33  
34  
35  
36  
37  
38  
39  
40  
41  
42  
43  
44  
45  
46  
47  
48  
49  
50  
51  
52  
53  
54  
55  
56  
57  
58  
59  
60  
The encapsulated specimen area was found to be relatively robust during prolonged STEM or TEM imaging  
at 80 kV, while unencapsulated areas were more beam sensitive. Enhanced resistance to beam-induced damage  
has been previously reported in thin molybdenum disulphide ( $\text{MoS}_2$ ) crystals when encapsulated by  
graphene.<sup>57-58</sup>

TEM imaging with electron energies above 80 kV is known to produce defects and holes in graphene and  
hBN, with both materials having similar electron beam damage thresholds.<sup>59</sup> Once a vacancy is formed, the  
under coordinated atoms surrounding the vacancy have lowered sputtering energy barriers, and are  
preferentially removed forming nanopores.<sup>60</sup> Although point defects and point defect clusters are impermeable

1  
2  
3 even to molecular He, theoretical calculations have found that water and oxygen can permeate graphene and  
4 hBN when pore diameters exceed  $\sim 1$  nm (as discussed in supplementary material section 4). We thus propose  
5 a novel two-stage process for patterning encapsulated BP flakes using the encapsulating flake as a ‘resist’  
6 layer. Firstly, a pattern is exposed using an electron beam, creating defects in the encapsulation layer.  
7  
8 Secondly, the sample is exposed to air, allowing oxidizing species to penetrate through the beam-induced holes  
9 and damage the BP crystal underneath, etching it to produce the exposed pattern. In common with direct write  
10 techniques<sup>43</sup>, combining this approach with electron diffraction allows flake patterning to be performed along  
11 specific crystallographic directions. Black phosphorus shows strong directional anisotropy in electronic<sup>14</sup> and  
12 thermal<sup>3</sup> transport due to its ridged structure, and therefore prior knowledge of the crystal orientation is  
13 invaluable when fabricating electronic devices to control transport behavior.  
14  
15  
16  
17  
18  
19  
20  
21  
22  
23  
24  
25  
26  
27  
28  
29  
30  
31  
32  
33  
34  
35  
36  
37  
38  
39  
40  
41  
42  
43  
44  
45  
46  
47  
48  
49  
50  
51  
52  
53  
54  
55  
56  
57  
58  
59  
60

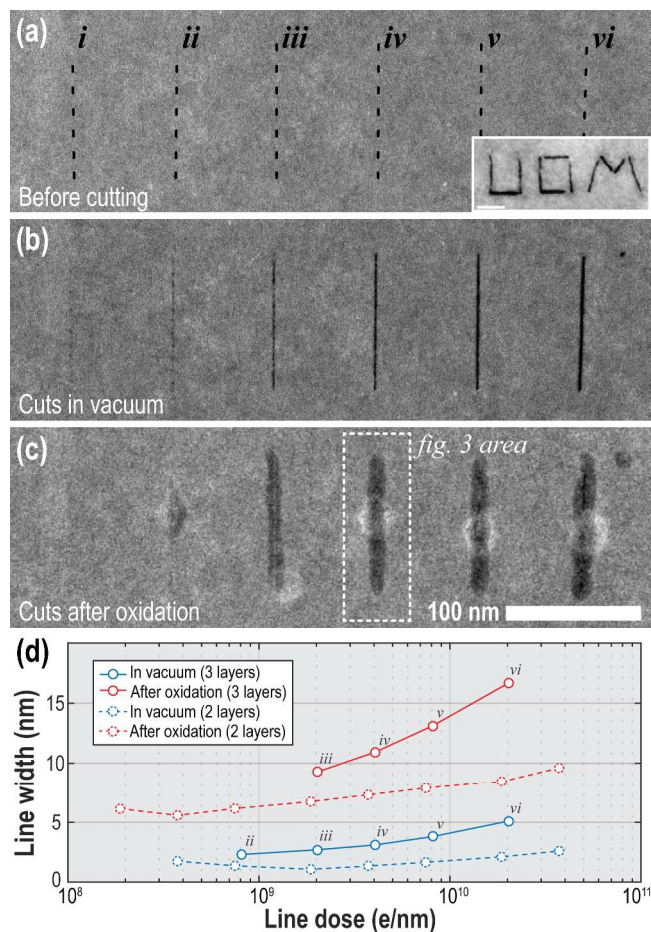


Figure 2: HAADF STEM images showing the controlled cutting of nm-resolution lines in an encapsulated (3 layer) BP flake. The width of the 100 nm long cuts is controlled by varying dwell time per pixel (i) 0.05, (ii) 0.1, (iii) 0.25, (iv) 0.5, (v) 1, and (vi) 2.5 seconds. Lines were drawn using a probe current of 1.3 nA, an accelerating voltage of 200 kV and 1 pixel/nm. (a) shows the area immediately prior to patterning. (b) shows the cuts immediately after patterning. (c) shows the same cuts after exposing sample to air at room temperature for 2 days. (d) The solid lines are a comparison of line widths on initial sculpting in the electron microscope (blue data) and after oxidation in air (red data) taken from the area shown in (a)-(c). The dashed lines show the change in line widths in a 2 layer sample as pictured in supporting material Figure S10. The inset in (a) is a demonstration of electron beam writing of “UOM” into a 10 nm thick BP crystal (scale bar: 20 nm).

To demonstrate local etching of BP we exposed a set of 100 nm long lines into a graphene encapsulated 3 layer BP crystal using a focused STEM probe, as shown in Figure 2. By progressively increasing the electron

1  
2  
3 dose used to make the cuts (pixel dwell-times varied between (i) 0.05 and (vi) 2.5 seconds with 100 pixels and  
4  
5 1.3nA beam current, 200 kV) we change the amount of damage induced which becomes clearly visible at the  
6  
7 dose of (iv)  $\sim 3 \times 10^9 \text{ e.nm}^{-1}$  as a clear cut approximately 3 nm wide through the entire BP film thickness. Further  
8  
9 increase in dose leads to effective broadening of the cut up to 5 nm at  $2 \times 10^{10} \text{ e.nm}^{-1}$ . We then exposed the  
10  
11 sample to air and ambient light for two days and repeated the imaging to find that the cuts have expanded  
12  
13 laterally and had identical contrast for all exposure doses above  $10^9 \text{ e.nm}^{-1}$ . The resulting line width was found  
14  
15 to be 6 -10 nm wider than before air contact giving the smallest feature size of 9 nm (for the 0.25s dwell time).  
16

17 We also patterned a series of 50 nm lines on a thinner encapsulated BP crystal (2 layers), with similar line  
18  
19 doses, as pictured in Supporting Material Figure S10, and achieved a smaller minimum feature size of 6 nm.  
20  
21 The line widths are plotted along with those from the 3 layer flake in Figure 2c. The difference in these two  
22  
23 measurements could be a result of the smaller flake thickness leading to a reduction in the electron beam  
24  
25 spreading and a resulting decrease in the damage region for the graphene, or to differences in the passivation  
26  
27 behavior for different BP layer thicknesses. However, we note that the difficulty of accurately focusing the  
28  
29 electron beam prior to etching, while simultaneously minimizing imaging of the sample to prevent unwanted  
30  
31 holes being created in the graphene sheet, could also affect the ultimate spatial resolution of the features we  
32  
33 observe.  
34

35 Importantly the dimensions of the damaged regions were found to be stable after initial air exposure and not  
36  
37 degrade further after several weeks' exposure to ambient conditions. This self-limiting etching behavior is  
38  
39 likely caused by a self-passivation process and we performed chemical mapping using EEL spectroscopy to  
40  
41 investigate this phenomena. By studying the total core-loss peak intensities, we estimate that in the center of  
42  
43 the cut feature the carbon and phosphorus intensities are reduced to around 50% and 35% of the surrounding  
44  
45 values respectively, indicating that most of the reaction products escape through the holes in the encapsulation  
46  
47 layer and a relatively small amount of material is left inside of the etched volume often collecting into pockets  
48  
49 (visible by increased contrast on Fig 2c). High resolution TEM and STEM revealed that the remaining material  
50  
51 is amorphous and volatile on exposure to the electron beam. A similar etching methodology was applied to  
52  
53 thicker samples and it was found to be possible to employ high beam currents to etch through the entire BP  
54  
55 thickness even for a  $\sim 10$  nm thick specimen (the 'UoM' inset from Figure 2).  
56  
57  
58  
59  
60

1  
2  
3 One of the key advantages of this patterning technique is that above a critical threshold, the shape of  
4 the patterned BP features is mostly invariant with the line dose used to pattern the encapsulating material.  
5 Whether we have created isolated defects with a pore size  $>\sim 5\text{\AA}$  (cut (ii) in Figure 2) separated by less than a  
6 few nm, or continuously penetrated both the BP flake and encapsulating layer (eg. cut (vi) in Figure 2), the  
7 self-passivating etching process means that resultant patterned BP area is remarkably similar. This means that,  
8 in contrast to conventional STEM sculpting of 2D materials<sup>61-63</sup>, the 2-step technique can be used to  
9 consistently pattern a large area, as the patterning behavior/resultant line width (in BP) is less dependent on the  
10 local level of surface contamination or the vacuum level. This effect also helps alleviate any difference in the  
11 TEM focus across a sample; the need to prevent the ‘unexposed’ areas from damage due to electron exposure  
12 means it is challenging to correctly focus the beam at the writing location, and minor focal differences can  
13 otherwise lead to significantly different patterning behavior. The fact that we completely penetrate through BP  
14 flakes up to 10nm thick and their encapsulating layers (inset, Fig 1), with similar spatial resolution as for the  
15 thin flakes, implies the 2-step technique is likely to be suitable for patterning even thicker flakes.  
16  
17  
18  
19  
20  
21  
22  
23  
24  
25  
26  
27  
28  
29  
30  
31  
32  
33  
34  
35  
36  
37  
38  
39  
40  
41  
42  
43  
44  
45  
46  
47  
48  
49  
50  
51  
52  
53  
54  
55  
56  
57  
58  
59  
60

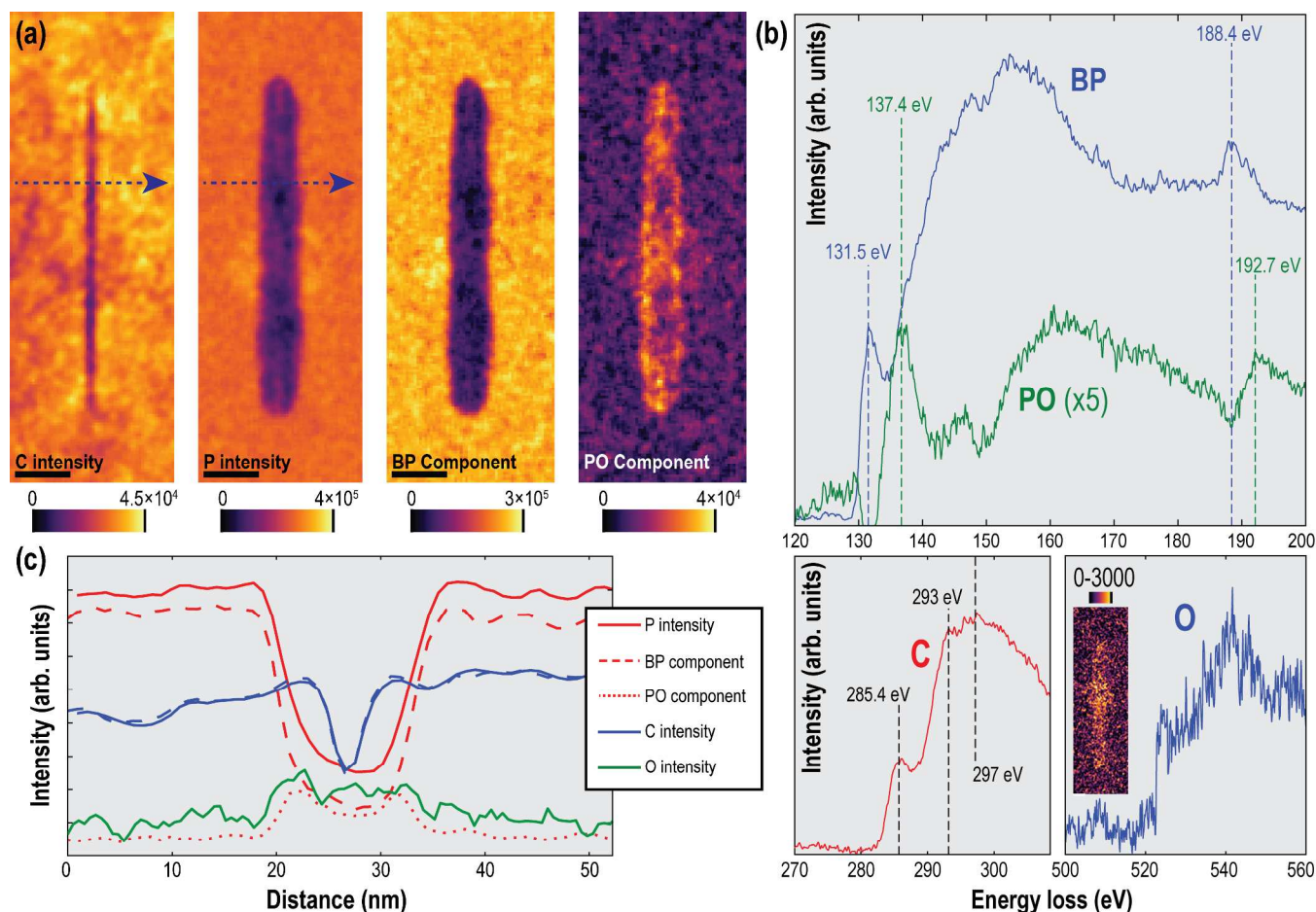


Figure 3: EEL spectrum imaging of the cut feature labelled (iv) in Figure 2c after oxidation. (a) Shows maps of the absolute intensity of the carbon K edge and the phosphorus L edges obtained by model based least squares fitting of the spectra at every pixel, along with maps of the components of the phosphorus L edges extracted using NMF algorithm corresponding to BP and oxidized phosphorus ( $P_xO_y$ ) (details of NMF decomposition in Supporting Material). Scale bars are 20 nm. (b) Shows the NMF factors corresponding to the BP and PO signals around the phosphorus L edges, as well as extracted carbon and oxygen K edges. The inset on the O K-edge plot is a map of the absolute intensity of the oxygen edge. (c) Shows the relative elemental intensities (shown by solid lines) along the profile indicated by the dotted line in (a). The dotted lines representing the separated BP and PO components are scaled by fitting their combined intensities to the elemental P intensity.

By performing non-negative matrix factorization<sup>64</sup> (NMF), the EEL spectra in the region of the phosphorus L edge was blindly separated into components corresponding to BP signals ( $L_{2,3}$  onset around 132 eV,  $L_1$  peak

1  
2  
3 around 188 eV)<sup>65-66</sup> and oxidized phosphorus, or P<sub>x</sub>O<sub>y</sub> (L<sub>2,3</sub> onset around 137 eV, L<sub>1</sub> peak around 193 eV).<sup>67</sup>  
4  
5 Details of the decomposition are presented in the supporting information, along with the individual NMF  
6  
7 components (in Figure S12). The BP and P<sub>x</sub>O<sub>y</sub> characteristic spectra, and the maps of their strength, are shown  
8  
9 in Figure 3. The P<sub>x</sub>O<sub>y</sub> signal is clearly maximized around the edges of the cut region, suggesting that a  
10  
11 passivating barrier has indeed been formed. Mapping of the carbon K edge indicates that the graphene sheets  
12  
13 have not been affected by the oxidation process, whilst oxygen K-edge mapping suggests an increased level of  
14  
15 elemental oxygen in the etched region, although the signal to noise ratio is too low to observe increased levels  
16  
17 around the edge, as suggested by the P<sub>x</sub>O<sub>y</sub> map.  
18

19 The ability of the BP to form a passivating oxide barrier along the edges of the cuts has important  
20  
21 implications. If the pattern is stable over time, we can employ the technique to define various electronic  
22  
23 structures (e.g. transistors, quantum dots, nanoribbons etc.) at an impressive resolution only limited by a  
24  
25 combination of the electron probe diameter and the thickness of the passivation layer. In order for this  
26  
27 approach to work the cuts must be electrically insulating.  
28

29 To test the electrical transport properties of our patterned structures, we have produced and selectively  
30  
31 oxidized two hBN encapsulated BP devices, with BP thicknesses of 2 and 4 layers respectively as measured  
32  
33 using the atomic force microscope (AFM). The lower encapsulating hBN layer had a thickness of ~20 nm, and  
34  
35 the upper hBN layer was a monolayer. After encapsulation the sample was transferred to a silicon wafer coated  
36  
37 with a 300 nm thick thermal oxide layer, to enable electrical gating of the BP. Gold was then deposited to  
38  
39 create high quality electrical contacts as described in our previous glovebox work.<sup>48</sup>  
40

41 Prior to the selective oxidation process, both devices demonstrated classical field effect behavior with hole  
42  
43 mobilities of 2000 cm<sup>2</sup>/Vs and 200 cm<sup>2</sup>/Vs for 4L and 2L respectively, similar to earlier reports<sup>48, 68</sup> on  
44  
45 encapsulated BP devices. We then used a 100 kV electron beam lithography instrument (Raith EBPG 5200) to  
46  
47 expose narrow lines across the conductive channel as indicated by the red lines in Figure 4 (a, b). After the  
48  
49 sample was exposed to ambient conditions, this exposure effectively separated contacts 2 and 3 from the rest  
50  
51 of the device with a low bias resistivity higher than 10<sup>8</sup> Ω, well above the 10<sup>3</sup> Ω value measured before the  
52  
53 etching procedure (Figure 4c). The realistic etched line width is estimated to be 12 nm taking into account the  
54  
55 4 nm pattern size exposed with a 2-3 nm beam diameter and including the 6 nm oxidation broadening. It is  
56  
57  
58  
59  
60

1  
2  
3 surprising that a gap only 12 nm wide spanning across 1  $\mu\text{m}$  sample size shows such a high resistivity at room  
4  
5 temperature (reproducible in both 2L and 4L devices). Furthermore, no leakage current was observed while  
6  
7 increasing the bias voltage up to 100 mV giving breakdown field of at least  $10^7$  V/m, better than that of  
8  
9 vacuum. While the etched regions of the sample changed their conductivity dramatically, other unexposed  
10  
11 areas (all other contacts) showed very little change, ruling out the possibility of accidental device degradation  
12  
13 between the measurements.  
14  
15  
16  
17  
18  
19  
20  
21  
22  
23  
24  
25  
26  
27  
28  
29  
30  
31  
32  
33  
34  
35  
36  
37  
38  
39  
40  
41  
42  
43  
44  
45  
46  
47  
48  
49  
50  
51  
52  
53  
54  
55  
56  
57  
58  
59  
60

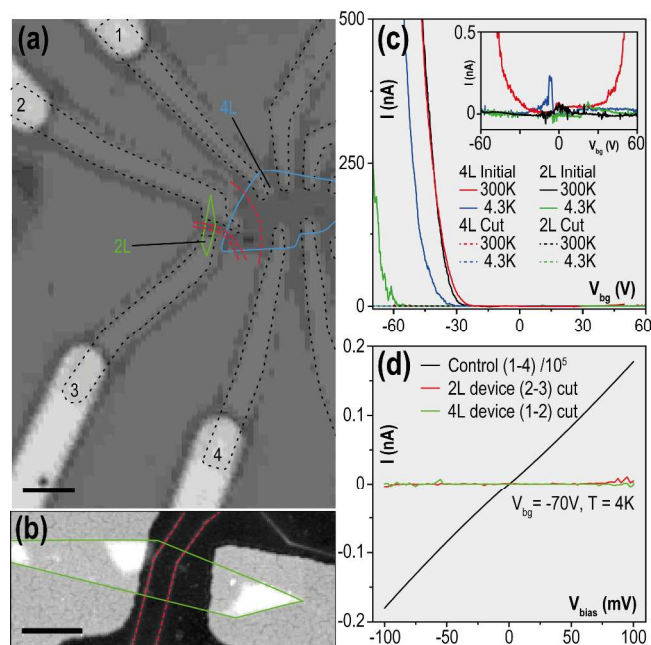


Figure 4: Electrical characterization of patterned few layer BP. (a) Optical micrograph of the device with multiple metallic contacts highlighted by black dashed line. Blue line shows edges of 4 layer BP flake (4L) and green line 2 layer BP flake (2L). Red lines indicate etched lines (b) AFM topography of the 2L device with crystal edges highlighted with green. (c) Electrical current measured in a two terminal configuration (between contacts 1-2 for the 4L flake and 2-3 for the 2L flake) before and after the etching procedure. The inset shows the dotted traces (voltages after patterning) with a reduced vertical scale to enhance visibility. (d) Current voltage characteristics measured across the 2L and 4L devices compared to unetched 4L sample (contacts 1-4). Scalebars (a)  $2\ \mu\text{m}$ , (b)  $500\ \text{nm}$ .

While fabricating such devices it was found to be especially important to avoid any areas which had pockets of trapped contamination - a common feature seen in heterostructures fabricated by the crystal stacking technique.<sup>47, 69</sup> In the STEM we observed that the action of the electron beam caused such contamination bubbles to etch down through the BP crystal (Figure S3 shows growth of such a hole at a dose rate of  $2500\ \text{e}\ \text{nm}^{-2}\ \text{s}^{-1}$ ). While the exact chemical composition of the trapped material inside the bubbles can vary depending on the techniques and conditions employed during the stacking procedure, we have previously shown that they contain hydrocarbon and oxygen species.<sup>69</sup> We hypothesize that these hydrocarbons are reduced to more chemically reactive species by the electron beam, which subsequently chemically etch the BP. After an

1  
2  
3 extended period of time the etching process appears to cease, after which the holes are stable for extended  
4 periods (as shown in Figures S4 and S5 in the supporting material). Electron diffraction and EEL spectrum  
5 imaging of this region indicate that crystalline phosphorus is entirely absent from the center of the hole  
6 although a small amount of oxidized phosphorus remains. The encapsulating graphene layers remain intact  
7 although we cannot rule out the presence of small holes. A ring of oxidized phosphorus ( $P_xO_y$ ) is seen around  
8 the edge of the hole, and outside this ring, no loss of crystallinity of the BP is observed. This suggests a similar  
9 self-passivation process to that which we observe for the etched lines, where the stable,  $P_xO_y$ , reaction product  
10 accumulates around the edge of the hole and prevents any further etching and which has been found to provide  
11 a passivation barrier for thicker BP flakes ( $>50$  nm)<sup>28</sup>. Similar behavior was observed in regions that had  
12 undergone high resolution TEM or STEM imaging, were then exposed to ambient conditions for up to 2.5  
13 months and then returned to the microscope (Figure S9 in the supporting information). Low dose and low  
14 accelerating voltage imaging conditions should therefore be employed to prevent the introduction of unwanted  
15 point defects while identifying the region of interest for pattern etching.  
16  
17  
18  
19  
20  
21  
22  
23  
24  
25  
26  
27  
28  
29

## 30 31 CONCLUSION

32  
33 In conclusion, we have developed a new method for nanometer scale patterning of few-layered BP.  
34 Encapsulation with graphene or hBN is found to provide an impermeable barrier which extends the long-term  
35 stability of few-layer BP crystals from a few minutes to at least several months, protecting it from  
36 environmental oxidation caused by the presence of light, air and moisture. By selectively damaging the  
37 encapsulating layer with an electron probe the protection is locally removed and subsequent exposure to  
38 ambient conditions causes etching of the BP crystal that extends 2-3 nm from the damaged region.  
39 Importantly, the patterned features are stable and do not expand during subsequent air contact due to  
40 passivation by oxygen-containing groups. With spatial resolutions of 6 nm readily achievable in few layer BP  
41 crystals, we demonstrate that features as narrow as 10 nm are already electrically insulating. This result  
42 highlights a potential route to harnessing the exciting properties of air-sensitive crystals in real applications.  
43 Minimizing levels of trapped contamination, and encapsulation with defect free graphene are likely to be  
44  
45  
46  
47  
48  
49  
50  
51  
52  
53  
54  
55  
56  
57  
58  
59  
60

1  
2  
3 critical factors for implementing this technique on a large scale and will require subsequent development of  
4 relevant fabrication and growth techniques.  
5  
6  
7

## 8 9 EXPERIMENTAL METHODS

### 10 11 **Device Fabrication**

12  
13 BP samples were mechanically exfoliated from bulk crystals (supplied by HQ Graphene) in an argon filled  
14 glovebox (oxygen and water levels below 0.1 ppm) onto a thin film of polypropylene carbonate (PPC). They  
15 were then immediately encapsulated using the van der Waals pickup technique, where the top encapsulating  
16 flake (supported by a PMMA membrane) is lowered onto the chosen BP flake, and used to slowly lift it away  
17 from the PPC substrate. The stack is then lowered onto the lower encapsulating flake. For the TEM/STEM  
18 samples, monolayer graphene was used as the encapsulation material, and the stack was transferred onto a  
19 Quantifoil or silicon nitride TEM support film, before the PMMA was removed by immersion in Acetone. The  
20 TEM support was then dried supercritically in a CO<sub>2</sub> atmosphere to prevent membrane damage due to the  
21 liquids surface tension. For the transport samples, hBN was used as the encapsulation material, with a  
22 monolayer piece on top, and a ~20 nm thick piece below. The stack was then transferred to a 290 nm thick  
23 oxidized silicon film supported by a silicon wafer, which acted as the back gate during transport  
24 measurements. Gold contacts were then fabricated using a lift off process after mask definition using EBL.  
25 Care was taken to avoid areas where trapped contamination bubbles were observed as these features caused  
26 unwanted local BP etching.  
27  
28  
29  
30  
31  
32  
33  
34  
35  
36  
37  
38  
39  
40

### 41 **TEM/STEM imaging**

42  
43 TEM and STEM analysis of the encapsulated BP was performed with a FEI Titan 80-200 ChemiSTEM with  
44 probe-side aberration correction at 200 kV and X-FEG electron source (Fig 2, Fig 3. Fig. S1-S3, S5 and S7-9).  
45 STEM experiments were performed with a 21 mrad convergence angle probe and probe current between 75 pA  
46 and 1.5nA. Whilst navigating to the region of interest for etching, low probe currents, low dwell times (1us)  
47 and low magnification were employed to minimize unwanted irradiation damage. The HAADF detector  
48 collected electrons scattered between 48 mrad and 191 mrad. EDX spectrum imaging was performed with a  
49 Super-X detector with a solid angle of ~0.7 sr. EEL spectra were acquired using a GIF Quantum with an  
50  
51  
52  
53  
54  
55  
56  
57  
58  
59  
60

1  
2  
3 energy dispersion of 0.25 eV and a collection angle of 38 mrad, providing an effective energy resolution of  
4  
5 1.75 eV. Complementary EELS data was also obtained from a Nion UltraSTEM100 aberration corrected  
6  
7 STEM operated at 60 kV with a beam current of 100 pA and showed similar features to that presented in Fig.  
8  
9 3. The cold field emission gun had an energy spread of 0.35 eV and core loss spectrum images were acquired  
10  
11 with a collection angle of 30 mrad. Aberration corrected TEM results were acquired on a JEOL ARM 200F at  
12  
13 an operating voltage of 80 kV (Fig 1). The BP flakes were found to be robust to prolonged STEM imaging at  
14  
15 200 kV over the acquisition time of 19 s, (total dose of  $\sim 47 \text{ e}\cdot\text{nm}^{-2}$  with a low dose rate of  $2.5 \text{ e}\cdot\text{nm}^{-2}\text{s}^{-1}$ ). The  
16  
17 encapsulated BP crystal structure also appears stable when imaged in TEM, showing little changes even after  
18  
19 extended atomic resolution imaging at 80 kV up to doses of  $2.6 \times 10^7 \text{ e}\cdot\text{nm}^{-2}$  and 200 kV up to doses of  $4.8 \times 10^6$   
20  
21  $\text{e}\cdot\text{nm}^{-2}$ . However, imaged regions subsequently degraded when removed from the microscope vacuum,  
22  
23 demonstrating that the graphene encapsulation had been damaged.

### 24 25 **TEM/STEM Analysis and Simulation**

26  
27 Principal Component Analysis (PCA) was performed on EELS spectrum imaging data using the Hyperspy  
28  
29 package to improve the signal to noise ratio.<sup>70-72</sup> For the EELS spectrum images shown in Figure 3, the non-  
30  
31 negative matrix factorization (NMF) algorithm packaged in Hyperspy was run on a section of the spectrum  
32  
33 image around the energy range of the phosphorus peak, after background removal and energy alignment using  
34  
35 the zero loss peak. The components were then visually divided into BP and PO components (components  
36  
37 pictured in Figure S12 in the supporting information), and summed to give reconstructed BP and  $\text{P}_x\text{O}_y$  spectra.  
38  
39 For Figure S8 in the supporting material, multiple linear least-squares regression (MLLS) was used to separate  
40  
41  $\text{P}_x\text{O}_y$  and BP peaks. Both analysis approaches showed the same qualitative results. Further in depth  
42  
43 consideration of the EELS analysis is provided in supplementary material section 5.

44  
45 TEM image simulation was performed using the JEMS software.<sup>73</sup> The settings for this simulation were  
46  
47 performed for a JEOL ARM200F: with accelerating voltage 80 kV;  $C_C$  1.2 mm;  $C_S$  -0.01 mm;  $C_5$ : 10 mm;  
48  
49 defocus: -8 nm and energy spread: 0.8 eV. The defocus spread was: 3 nm.

### 50 51 **Patterning Parameters**

52  
53 Lines were exposed in suspended graphene encapsulated hBN flakes using a FEI Titan 80-200 ChemiSTEM  
54  
55 with a 200 kV accelerating voltage. Beam currents up to 1.3 nA were used, with a step size of 1 nm per pixel  
56  
57  
58  
59  
60

1  
2  
3 and the pixel dwell time was varied, giving total line doses between 0.2-2 nC/nm. For EBL thin BP areas were  
4 exposed in hBN encapsulated flakes using a 100 keV Raith EBPG 5200. A beam current of 200 pA was used,  
5 with a step size of 0.85 nm per pixel and a pattern width of 4.25 nm. The dwell time was chosen to give a total  
6 area dose of 1 C/cm<sup>2</sup>.  
7  
8  
9

### 10 11 12 ASSOCIATED CONTENT

13  
14 Supporting information is available free of charge on the ACS publications website at DOI, containing  
15 supplementary images showing: optical images of additional TEM samples, details of BP thickness  
16 determination using diffraction images, etching of contamination induced hole during electron illumination,  
17 low magnification images showing distribution of contamination pockets, EEL spectrum imaging of a  
18 contamination induced hole, EDX spectral imaging and selected area diffraction imaging of a BP oxidation  
19 feature caused by previous high mag STEM imaging, HAADF images of etched lines in 2 layer BP, NMF  
20 components used to separate BP and P<sub>x</sub>O<sub>y</sub> signals in Figure 3, EELS spectrum imaging of a wider area  
21 showing all cuts from Figure 2, and justification of choice of factor number for NMF decomposition for EEL  
22 spectrum images. All raw data is available from the corresponding authors on request.  
23  
24  
25  
26  
27  
28  
29  
30  
31  
32

### 33 AUTHOR INFORMATION

34 Corresponding Author

35  
36 [\\*sarah.haigh@manchester.ac.uk](mailto:*sarah.haigh@manchester.ac.uk); [+roman@manchester.ac.uk](mailto:+roman@manchester.ac.uk)

37  
38 Author Contributions

39  
40 RVG, YC, MH and NC made the samples. LN, EAL, EP, RK, JS, DK, AG and SJH performed the STEM  
41 experiments. RVG, FS and MZ performed the EBL experiments. LN, NC, RVG and SJH wrote the  
42 manuscript, all authors contributed to analyzing the data and interpreting the results  
43  
44  
45  
46

47 Funding Sources

48  
49 The authors would like to thank the Engineering and Physical Sciences (EPSRC) U.K Grants  
50 EP/G035954/1, EP/K016946/1, EP/J021172/1 and EP/P009050/1, the NowNANO Graphene CDT, and the  
51 Defense Threat Reduction Agency Grant HDTRA1-12-1-0013 for funding. Access to aberration corrected  
52 electron microscopy was provided through the EPSRC SuperSTEM laboratory. FS acknowledges funding  
53  
54  
55  
56  
57  
58  
59  
60

1  
2  
3 from the European Graphene Flagship Project and the European Research Council through the Hetero2D  
4 Synergy grant. SJH acknowledges funding European Research Council (ERC) under the European Union's  
5 Horizon 2020 research and innovation programme (Grant Agreement ERC-2016-STG-EvoluTEM-715502).  
6  
7  
8  
9 RVG acknowledges the Royal Society Fellowship scheme.

#### 11 Notes

12  
13 The authors declare no competing financial interest.

#### 17 REFERENCES

- 19  
20 (1) Churchill, H.O.;Jarillo-Herrero, P. Two-Dimensional Crystals: Phosphorus Joins the Family.  
21 *Nat. Nanotechnol.* **2014**, *9* (5), 330-1.  
22 (2) Liu, H.; Du, Y.; Deng, Y.;Ye, P.D. Semiconducting Black Phosphorus: Synthesis, Transport  
23 Properties and Electronic Applications. *Chem. Soc. Rev.* **2015**, *44* (9), 2732-43.  
24 (3) Ling, X.; Wang, H.; Huang, S.; Xia, F.;Dresselhaus, M.S. The Renaissance of Black  
25 Phosphorus. *Proc. Natl. Acad. Sci. U.S.A.* **2015**, *112* (15), 4523-30.  
26 (4) Castellanos-Gomez, A.; Vicarelli, L.; Prada, E.; Island, J.O.; Narasimha-Acharya, K.L.;  
27 Blanter, S.I.; Groenendijk, D.J.; Buscema, M.; Steele, G.A.; Alvarez, J.V.; Zandbergen, H.W.;  
28 Palacios, J.J.;van der Zant, H.S.J. Isolation and Characterization of Few-Layer Black  
29 Phosphorus. *2D Mater.* **2014**, *1* (2), 025001.  
30 (5) Li, L.; Yu, Y.; Ye, G.J.; Ge, Q.; Ou, X.; Wu, H.; Feng, D.; Chen, X.H.;Zhang, Y. Black  
31 Phosphorus Field-Effect Transistors. *Nat. Nanotechnol.* **2014**, *9* (5), 372-7.  
32 (6) Koenig, S.P.; Doganov, R.A.; Schmidt, H.; Neto, A.H.C.;Ozyilmaz, B. Electric Field Effect  
33 in Ultrathin Black Phosphorus. *Appl. Phys. Lett.* **2014**, *104* (10).  
34 (7) Brent, J.R.; Savjani, N.; Lewis, E.A.; Haigh, S.J.; Lewis, D.J.;O'Brien, P. Production of Few-  
35 Layer Phosphorene by Liquid Exfoliation of Black Phosphorus. *Chem. Commun. (Cambridge,*  
36 *U.K.)* **2014**, *50* (87), 13338-41.  
37 (8) Hanlon, D.; Backes, C.; Doherty, E.; Cucinotta, C.S.; Berner, N.C.; Boland, C.; Lee, K.;  
38 Harvey, A.; Lynch, P.; Gholamvand, Z.; Zhang, S.; Wang, K.; Moynihan, G.; Pokle, A.;  
39 Ramasse, Q.M.; McEvoy, N.; Blau, W.J.; Wang, J.; Abellan, G.; Hauke, F.; Hirsch, A.; Sanvito,  
40 S.; O'Regan, D.D.; Duesberg, G.S.; Nicolosi, V.;Coleman, J.N. Liquid Exfoliation of Solvent-  
41 Stabilized Few-Layer Black Phosphorus for Applications Beyond Electronics. *Nat Commun*  
42 **2015**, *6*, 8563.  
43 (9) Lewis, E.A.; Brent, J.R.; Derby, B.; Haigh, S.J.;Lewis, D.J. Solution Processing of Two-  
44 Dimensional Black Phosphorus. *Chem. Commun. (Cambridge, U.K.)* **2017**, *53* (9), 1445-1458.  
45 (10) Liu, H.; Neal, A.T.; Zhu, Z.; Luo, Z.; Xu, X.; Tomanek, D.;Ye, P.D. Phosphorene: An  
46 Unexplored 2d Semiconductor with a High Hole Mobility. *ACS Nano* **2014**, *8* (4), 4033-41.  
47 (11) Tran, V.; Soklaski, R.; Liang, Y.F.;Yang, L. Layer-Controlled Band Gap and Anisotropic  
48 Excitons in Few-Layer Black Phosphorus. *Phys. Rev. B* **2014**, *89* (23).  
49 (12) Das, S.; Zhang, W.; Demarteau, M.; Hoffmann, A.; Dubey, M.;Roelofs, A. Tunable  
50 Transport Gap in Phosphorene. *Nano Lett.* **2014**, *14* (10), 5733-9.  
51  
52  
53  
54  
55  
56  
57  
58  
59  
60

- 1  
2  
3 (13) Keyes, R.W. The Electrical Properties of Black Phosphorus. *Phys. Rev.* **1953**, *92* (3), 580-  
4 584.
- 5 (14) Qiao, J.; Kong, X.; Hu, Z.X.; Yang, F.; Ji, W. High-Mobility Transport Anisotropy and  
6 Linear Dichroism in Few-Layer Black Phosphorus. *Nat. Commun.* **2014**, *5*, 4475.
- 7 (15) Long, G.; Maryenko, D.; Shen, J.; Xu, S.; Hou, J.; Wu, Z.; Wong, W.K.; Han, T.; Lin, J.;  
8 Cai, Y.; Lortz, R.; Wang, N. Achieving Ultrahigh Carrier Mobility in Two-Dimensional Hole Gas  
9 of Black Phosphorus. *Nano Lett.* **2016**, *16* (12), 7768-7773.
- 10 (16) Gillgren, N.; Wickramaratne, D.; Shi, Y.M.; Espiritu, T.; Yang, J.W.; Hu, J.; Wei, J.; Liu,  
11 X.; Mao, Z.Q.; Watanabe, K.; Taniguchi, T.; Bockrath, M.; Barlas, Y.; Lake, R.K.; Lau, C.N.  
12 Gate Tunable Quantum Oscillations in Air-Stable and High Mobility Few-Layer Phosphorene  
13 Heterostructures. *2D Mater.* **2015**, *2* (1), 011001.
- 14 (17) Xia, F.; Wang, H.; Jia, Y. Rediscovering Black Phosphorus as an Anisotropic Layered  
15 Material for Optoelectronics and Electronics. *Nat. Commun.* **2014**, *5*, 4458.
- 16 (18) Buscema, M.; Groenendijk, D.J.; Blanter, S.I.; Steele, G.A.; van der Zant, H.S.; Castellanos-  
17 Gomez, A. Fast and Broadband Photoresponse of Few-Layer Black Phosphorus Field-Effect  
18 Transistors. *Nano Lett.* **2014**, *14* (6), 3347-52.
- 19 (19) Engel, M.; Steiner, M.; Avouris, P. Black Phosphorus Photodetector for Multispectral,  
20 High-Resolution Imaging. *Nano Lett.* **2014**, *14* (11), 6414-7.
- 21 (20) Low, T.; Rodin, A.S.; Carvalho, A.; Jiang, Y.J.; Wang, H.; Xia, F.N.; Neto, A.H.C. Tunable  
22 Optical Properties of Multilayer Black Phosphorus Thin Films. *Phys. Rev. B* **2014**, *90* (7).
- 23 (21) Ferrari, A.C.; Bonaccorso, F.; Fal'ko, V.; Novoselov, K.S.; Roche, S.; Boggild, P.; Borini,  
24 S.; Koppens, F.H.; Palermo, V.; Pugno, N.; Garrido, J.A.; Sordan, R.; Bianco, A.; Ballerini, L.;  
25 Prato, M.; Lidorikis, E.; Kivioja, J.; Marinelli, C.; Ryhanen, T.; Morpurgo, A.; Coleman, J.N.;  
26 Nicolosi, V.; Colombo, L.; Fert, A.; Garcia-Hernandez, M.; Bachtold, A.; Schneider, G.F.;  
27 Guinea, F.; Dekker, C.; Barbone, M.; Sun, Z.; Galiotis, C.; Grigorenko, A.N.; Konstantatos, G.;  
28 Kis, A.; Katsnelson, M.; Vandersypen, L.; Loiseau, A.; Morandi, V.; Neumaier, D.; Treossi, E.;  
29 Pellegrini, V.; Polini, M.; Tredicucci, A.; Williams, G.M.; Hong, B.H.; Ahn, J.H.; Kim, J.M.;  
30 Zirath, H.; van Wees, B.J.; van der Zant, H.; Occhipinti, L.; Di Matteo, A.; Kinloch, I.A.;  
31 Seyller, T.; Quesnel, E.; Feng, X.; Teo, K.; Rupesinghe, N.; Hakonen, P.; Neil, S.R.; Tannock,  
32 Q.; Lofwander, T.; Kinaret, J. Science and Technology Roadmap for Graphene, Related Two-  
33 Dimensional Crystals, and Hybrid Systems. *Nanoscale* **2015**, *7* (11), 4598-810.
- 34 (22) Favron, A.; Gaufres, E.; Fossard, F.; Phaneuf-L'Heureux, A.L.; Tang, N.Y.; Levesque,  
35 P.L.; Loiseau, A.; Leonelli, R.; Francoeur, S.; Martel, R. Photooxidation and Quantum  
36 Confinement Effects in Exfoliated Black Phosphorus. *Nat. Mater.* **2015**, *14* (8), 826-32.
- 37 (23) Hanlon, D.; Backes, C.; Doherty, E.; Cucinotta, C.S.; Berner, N.C.; Boland, C.; Lee, K.;  
38 Harvey, A.; Lynch, P.; Gholamvand, Z.; Zhang, S.; Wang, K.; Moynihan, G.; Pokle, A.;  
39 Ramasse, Q.M.; McEvoy, N.; Blau, W.J.; Wang, J.; Abellan, G.; Hauke, F.; Hirsch, A.; Sanvito,  
40 S.; O'Regan, D.D.; Duesberg, G.S.; Nicolosi, V.; Coleman, J.N. Liquid Exfoliation of Solvent-  
41 Stabilized Few-Layer Black Phosphorus for Applications Beyond Electronics. *Nat. Commun.*  
42 **2015**, *6*, 8563.
- 43 (24) Island, J.O.; Steele, G.A.; van der Zant, H.S.J.; Castellanos-Gomez, A. Environmental  
44 Instability of Few-Layer Black Phosphorus. *2D Mater.* **2015**, *2* (1), 011002.
- 45 (25) Wood, J.D.; Wells, S.A.; Jariwala, D.; Chen, K.S.; Cho, E.; Sangwan, V.K.; Liu, X.;  
46 Lauhon, L.J.; Marks, T.J.; Hersam, M.C. Effective Passivation of Exfoliated Black Phosphorus  
47 Transistors against Ambient Degradation. *Nano Lett.* **2014**, *14* (12), 6964-70.
- 48  
49  
50  
51  
52  
53  
54  
55  
56  
57  
58  
59  
60

- (26) Abellan, G.; Wild, S.; Lloret, V.; Scheuschner, N.; Gillen, R.; Mundloch, U.; Maultzsch, J.; Varela, M.; Hauke, F.; Hirsch, A. Fundamental Insights into the Degradation and Stabilization of Thin Layer Black Phosphorus. *J. Am. Chem. Soc.* **2017**, *139* (30), 10432-10440.
- (27) Yau, S.L.; Moffat, T.P.; Bard, A.J.; Zhang, Z.W.; Lerner, M.M. STM of the (010) Surface of Orthorhombic Phosphorus. *Chem. Phys. Lett.* **1992**, *198* (3-4), 383-388.
- (28) Edmonds, M.T.; Tadich, A.; Carvalho, A.; Ziletti, A.; O'Donnell, K.M.; Koenig, S.P.; Coker, D.F.; Ozyilmaz, B.; Neto, A.H.; Fuhrer, M.S. Creating a Stable Oxide at the Surface of Black Phosphorus. *ACS Appl. Mater. Interfaces* **2015**, *7* (27), 14557-62.
- (29) Pei, J.J.; Gai, X.; Yang, J.; Wang, X.B.; Yu, Z.F.; Choi, D.Y.; Luther-Davies, B.; Lu, Y.R. Producing Air-Stable Monolayers of Phosphorene and Their Defect Engineering. *Nat. Commun.* **2016**, *7*, 10450.
- (30) Kim, J.S.; Liu, Y.; Zhu, W.; Kim, S.; Wu, D.; Tao, L.; Dodabalapur, A.; Lai, K.; Akinwande, D. Toward Air-Stable Multilayer Phosphorene Thin-Films and Transistors. *Sci. Rep.* **2015**, *5*, 8989.
- (31) Na, J.; Lee, Y.T.; Lim, J.A.; Hwang, D.K.; Kim, G.T.; Choi, W.K.; Song, Y.W. Few-Layer Black Phosphorus Field-Effect Transistors with Reduced Current Fluctuation. *ACS Nano* **2014**, *8* (11), 11753-62.
- (32) Miyeon, L.; Arup Kumer, R.; Seongho, J.; Yujin, C.; Ari, C.; Bongsoo, K.; Sung Yong, P.; Insik, I. Exfoliation of Black Phosphorus in Ionic Liquids. *Nanotechnology* **2017**, *28* (12), 125603.
- (33) Chaban, V.V.; Fileti, E.E.; Prezhdo, O.V. Imidazolium Ionic Liquid Mediates Black Phosphorus Exfoliation While Preventing Phosphorene Decomposition. *ACS Nano* **2017**, *11* (6), 6459-6466.
- (34) Doganov, R.A.; O'Farrell, E.C.; Koenig, S.P.; Yeo, Y.; Ziletti, A.; Carvalho, A.; Campbell, D.K.; Coker, D.F.; Watanabe, K.; Taniguchi, T.; Castro Neto, A.H.; Ozyilmaz, B. Transport Properties of Pristine Few-Layer Black Phosphorus by Van Der Waals Passivation in an Inert Atmosphere. *Nat. Commun.* **2015**, *6*, 6647.
- (35) Avsar, A.; Vera-Marun, I.J.; Tan, J.Y.; Watanabe, K.; Taniguchi, T.; Castro Neto, A.H.; Ozyilmaz, B. Air-Stable Transport in Graphene-Contacted, Fully Encapsulated Ultrathin Black Phosphorus-Based Field-Effect Transistors. *ACS Nano* **2015**, *9* (4), 4138-45.
- (36) Avsar, A.; Tan, J.Y.; Luo, X.; Khoo, K.H.; Yeo, Y.; Watanabe, K.; Taniguchi, T.; Quek, S.Y.; Ozyilmaz, B. Van Der Waals Bonded Co/H-Bn Contacts to Ultrathin Black Phosphorus Devices. *Nano Lett.* **2017**, *17* (9), 5361-5367.
- (37) Hu, S.; Lozada-Hidalgo, M.; Wang, F.C.; Mishchenko, A.; Schedin, F.; Nair, R.R.; Hill, E.W.; Boukhvalov, D.W.; Katsnelson, M.I.; Dryfe, R.A.; Grigorieva, I.V.; Wu, H.A.; Geim, A.K. Proton Transport through One-Atom-Thick Crystals. *Nature* **2014**, *516* (7530), 227-30.
- (38) Guo, H.Y.; Lu, N.; Dai, J.; Wu, X.J.; Zeng, X.C. Phosphorene Nanoribbons, Phosphorus Nanotubes, and Van Der Waals Multilayers. *J. Phys. Chem. C* **2014**, *118* (25), 14051-14059.
- (39) Peng, X.H.; Coppole, A.; Wei, Q. Edge Effects on the Electronic Properties of Phosphorene Nanoribbons. *J. Appl. Phys.* **2014**, *116* (14), 144301.
- (40) Ramasubramaniam, A.; Muniz, A.R. Ab Initio Studies of Thermodynamic and Electronic Properties of Phosphorene Nanoribbons. *Phys. Rev. B* **2014**, *90* (8), 085424.
- (41) Tran, V.; Yang, L. Scaling Laws for the Band Gap and Optical Response of Phosphorene Nanoribbons. *Phys. Rev. B* **2014**, *89* (24), 245407.

- (42) Zhang, J.; Liu, H.J.; Cheng, L.; Wei, J.; Liang, J.H.; Fan, D.D.; Shi, J.; Tang, X.F.; Zhang, Q.J. Phosphorene Nanoribbon as a Promising Candidate for Thermoelectric Applications. *Sci. Rep.* **2014**, *4*, 6452.
- (43) Masih Das, P.; Danda, G.; Cupo, A.; Parkin, W.M.; Liang, L.; Kharche, N.; Ling, X.; Huang, S.; Dresselhaus, M.S.; Meunier, V.; Drndic, M. Controlled Sculpture of Black Phosphorus Nanoribbons. *ACS Nano* **2016**, *10* (6), 5687-95.
- (44) Cupo, A.; Masih Das, P.; Chien, C.C.; Danda, G.; Kharche, N.; Tristant, D.; Drndic, M.; Meunier, V. Periodic Arrays of Phosphorene Nanopores as Antidot Lattices with Tunable Properties. *ACS Nano* **2017**, *11* (7), 7494-7507.
- (45) Pizzocchero, F.; Gammelgaard, L.; Jessen, B.S.; Caridad, J.M.; Wang, L.; Hone, J.; Boggild, P.; Booth, T.J. The Hot Pick-up Technique for Batch Assembly of Van Der Waals Heterostructures. *Nat. Commun.* **2016**, *7*, 11894.
- (46) Frisenda, R.; Navarro-Moratalla, E.; Gant, P.; Perez De Lara, D.; Jarillo-Herrero, P.; Gorbachev, R.V.; Castellanos-Gomez, A. Recent Progress in the Assembly of Nanodevices and Van Der Waals Heterostructures by Deterministic Placement of 2d Materials. *Chem. Soc. Rev.* **2018**, *47* (1), 53-68.
- (47) Kretinin, A.V.; Cao, Y.; Tu, J.S.; Yu, G.L.; Jalil, R.; Novoselov, K.S.; Haigh, S.J.; Gholinia, A.; Mishchenko, A.; Lozada, M.; Georgiou, T.; Woods, C.R.; Withers, F.; Blake, P.; Eda, G.; Wirsig, A.; Hucho, C.; Watanabe, K.; Taniguchi, T.; Geim, A.K.; Gorbachev, R.V. Electronic Properties of Graphene Encapsulated with Different Two-Dimensional Atomic Crystals. *Nano Lett.* **2014**, *14* (6), 3270-6.
- (48) Cao, Y.; Mishchenko, A.; Yu, G.L.; Khestanova, E.; Rooney, A.P.; Prestat, E.; Kretinin, A.V.; Blake, P.; Shalom, M.B.; Woods, C.; Chapman, J.; Balakrishnan, G.; Grigorieva, I.V.; Novoselov, K.S.; Piot, B.A.; Potemski, M.; Watanabe, K.; Taniguchi, T.; Haigh, S.J.; Geim, A.K.; Gorbachev, R.V. Quality Heterostructures from Two-Dimensional Crystals Unstable in Air by Their Assembly in Inert Atmosphere. *Nano Lett.* **2015**, *15* (8), 4914-21.
- (49) Bandurin, D.A.; Tyurnina, A.V.; Yu, G.L.; Mishchenko, A.; Zolyomi, V.; Morozov, S.V.; Kumar, R.K.; Gorbachev, R.V.; Kudrynskiy, Z.R.; Pezzini, S.; Kovalyuk, Z.D.; Zeitler, U.; Novoselov, K.S.; Patane, A.; Eaves, L.; Grigorieva, I.V.; Fal'ko, V.I.; Geim, A.K.; Cao, Y. High Electron Mobility, Quantum Hall Effect and Anomalous Optical Response in Atomically Thin Inse. *Nat. Nanotechnol.* **2017**, *12* (3), 223-227.
- (50) Chen, H.; Fei, W.; Zhou, J.; Miao, C.; Guo, W. Layer Identification of Colorful Black Phosphorus. *Small* **2017**, *13* (5), 1602336.
- (51) Blake, P.; Hill, E.W.; Castro Neto, A.H.; Novoselov, K.S.; Jiang, D.; Yang, R.; Booth, T.J.; Geim, A.K. Making Graphene Visible. *Appl. Phys. Lett.* **2007**, *91* (6), 063124.
- (52) Castellanos-Gomez, A.; Agrait, N.; Rubio-Bollinger, G. Optical Identification of Atomically Thin Dichalcogenide Crystals. *Appl. Phys. Lett.* **2010**, *96* (21).
- (53) Hultgren, R.; Gingrich, N.S.; Warren, B.E. The Atomic Distribution in Red and Black Phosphorus and the Crystal Structure of Black Phosphorus. *J. Chem. Phys.* **1935**, *3* (6), 351-355.
- (54) Maruyama, Y.; Suzuki, S.; Kobayashi, K.; Tanuma, S. Synthesis and Some Properties of Black Phosphorus Single-Crystals. *Physica B & C* **1981**, *105* (1-3), 99-102.
- (55) Shirotani, I. Growth of Large Single-Crystals of Black Phosphorus at High-Pressures and Temperatures, and Its Electrical-Properties. *Mol. Cryst. Liq. Cryst.* **1982**, *86* (1-4), 1943-1951.
- (56) Morita, A. Semiconducting Black Phosphorus. *Appl. Phys. A* **1986**, *39* (4), 227-242.
- (57) Zan, R.; Ramasse, Q.M.; Jalil, R.; Georgiou, T.; Bangert, U.; Novoselov, K.S. Control of Radiation Damage in Mos(2) by Graphene Encapsulation. *ACS Nano* **2013**, *7* (11), 10167-74.

(58) Algara-Siller, G.; Kurasch, S.; Sedighi, M.; Lehtinen, O.; Kaiser, U. The Pristine Atomic Structure of Mos2 Monolayer Protected from Electron Radiation Damage by Graphene (Vol 103, 203107, 2013). *Appl. Phys. Lett.* **2013**, *103* (23).

(59) Kotakoski, J.; Jin, C.H.; Lehtinen, O.; Suenaga, K.; Krasheninnikov, A.V. Electron Knock-on Damage in Hexagonal Boron Nitride Monolayers. *Phys. Rev. B* **2010**, *82* (11), 113404.

(60) Warner, J.H.; Rummeli, M.H.; Bachmatiuk, A.; Buchner, B. Atomic Resolution Imaging and Topography of Boron Nitride Sheets Produced by Chemical Exfoliation. *ACS Nano* **2010**, *4* (3), 1299-304.

(61) Bornert, F.; Fu, L.; Gorantla, S.; Knupfer, M.; Buchner, B.; Rummeli, M.H. Programmable Sub-Nanometer Sculpting of Graphene with Electron Beams. *ACS Nano* **2012**, *6* (11), 10327-34.

(62) Fischbein, M.D.; Drndic, M. Electron Beam Nanosculpting of Suspended Graphene Sheets. *Appl. Phys. Lett.* **2008**, *93* (11), 113107.

(63) Song, B.; Schneider, G.F.; Xu, Q.; Pandraud, G.; Dekker, C.; Zandbergen, H. Atomic-Scale Electron-Beam Sculpting of near-Defect-Free Graphene Nanostructures. *Nano Lett.* **2011**, *11* (6), 2247-50.

(64) Nicoletti, O.; de la Pena, F.; Leary, R.K.; Holland, D.J.; Ducati, C.; Midgley, P.A. Three-Dimensional Imaging of Localized Surface Plasmon Resonances of Metal Nanoparticles. *Nature* **2013**, *502* (7469), 80-4.

(65) Nicotra, G.; Politano, A.; Mio, A.M.; Deretzis, I.; Hu, J.; Mao, Z.Q.; Wei, J.; La Magna, A.; Spinella, C. Absorption Edges of Black Phosphorus: A Comparative Analysis. *Phys. Status Solidi B* **2016**, *253* (12), 2509-2514.

(66) Abdolmaleki, A.; Dadsetani, M. Excitonic Effects in the K and L 2,3 Edges Spectra of Bulk and Monolayer Black Phosphorus from First-Principles. *J. Electron. Spectrosc. Relat. Phenom.* **2018**, *223*, 1-10.

(67) Kruse, J.; Leinweber, P.; Eckhardt, K.U.; Godlinski, F.; Hu, Y.; Zuin, L. Phosphorus L(2,3)-Edge Xanes: Overview of Reference Compounds. *J. Synchrotron Radiat.* **2009**, *16* (Pt 2), 247-59.

(68) Chen, X.; Wu, Y.; Wu, Z.; Han, Y.; Xu, S.; Wang, L.; Ye, W.; Han, T.; He, Y.; Cai, Y.; Wang, N. High-Quality Sandwiched Black Phosphorus Heterostructure and Its Quantum Oscillations. *Nat. Commun.* **2015**, *6*, 7315.

(69) Haigh, S.J.; Gholinia, A.; Jalil, R.; Romani, S.; Britnell, L.; Elias, D.C.; Novoselov, K.S.; Ponomarenko, L.A.; Geim, A.K.; Gorbachev, R. Cross-Sectional Imaging of Individual Layers and Buried Interfaces of Graphene-Based Heterostructures and Superlattices. *Nat. Mater.* **2012**, *11* (9), 764-7.

(70) Arenal, R.; de la Pena, F.; Stephan, O.; Walls, M.; Tence, M.; Loiseau, A.; Colliex, C. Extending the Analysis of EELS Spectrum-Imaging Data, from Elemental to Bond Mapping in Complex Nanostructures. *Ultramicroscopy* **2008**, *109* (1), 32-8.

(71) Trebbia, P.; Bonnet, N. EELS Elemental Mapping with Unconventional Methods. I. Theoretical Basis: Image Analysis with Multivariate Statistics and Entropy Concepts. *Ultramicroscopy* **1990**, *34* (3), 165-78.

(72) Peña, F.D.L.; Ostasevicius, T.; Fauske, V.T.; Burdet, P.; Jokubauskas, P.; Nord, M.; Prestat, E.; Sarahan, M.; MacArthur, K.E.; Johnstone, D.N.; Taillon, J.; Caron, J.; Furnival, T.; Eljarrat, A.; Mazzucco, S.; Migunov, V.; Aarholt, T.; Walls, M.; Winkler, F.; Martineau, B.; Donval, G.; Høglund, E.R.; Alxneit, I.; Hjorth, I.; Zagonel, L.F.; Garmannslund, A.; Gohlke, C.; Iyengar, I.; Chang, H.-W. *Hyperspy/Hyperspy: Hyperspy 1.3*, **2017**, 10.5281/ZENODO.583693.

1  
2  
3 (73) Stadelmann, P.A. Ems - a Software Package for Electron-Diffraction Analysis and Hrem  
4 Image Simulation in Materials Science. *Ultramicroscopy* **1987**, *21* (2), 131-145.  
5  
6  
7  
8  
9  
10  
11  
12  
13  
14  
15  
16  
17  
18  
19  
20  
21  
22  
23  
24  
25  
26  
27  
28  
29  
30  
31  
32  
33  
34  
35  
36  
37  
38  
39  
40  
41  
42  
43  
44  
45  
46  
47  
48  
49  
50  
51  
52  
53  
54  
55  
56  
57  
58  
59  
60

## TOC Graphic

